J|A|C|S
ARTICLES
Published on Web 05/02/2006

^{1}H NMR Study of the Magnetic Properties and Electronic Structure of the Hydroxide Complex of Substrate-bound Heme Oxygenase from *Neisseria Meningitidis*: Influence of the Axial Water Deprotonation on the Distal H-bond Network

Li-Hua Ma,[†] Yangzhong Liu,[†] Xuhang Zhang,[‡] Tadashi Yoshida,[‡] and Gerd N. La Mar*,[†]

Contribution from the Department of Chemistry, University of California, Davis, California 95616 and Department of Biochemistry, Yamagata University School of Medicine, Yamagata 990-9585, Japan

Received December 29, 2005; E-mail: lamar@chem.ucdavis.edu

Abstract: The substrate and active site residues of the low-spin hydroxide complex of the protohemin complex of *Neisseria meningitidis* heme oxygenase (*Nm*HO) have been assigned by saturation transfer between the hydroxide and previously characterized aquo complex. The available dipolar shifts allowed the quantitation of both the orientation and anisotropy of the paramagnetic susceptibility tensor. The resulting positive sign, and reduced magnitude of the axial anisotropy relative to the cyanide complex, dictate that the orbital ground state is the conventional "d_π" ($d^2_{xy}(d_{xz}, d_{yz})^3$); and not the unusual "$d_{xy}$" ($d^2_{xz}d^2_{yz}d_{xy}$) orbital ground state reported for the hydroxide complex of the homologous heme oxygenase (HO) from *Pseudomonas aeruginosa* (Caignan, G.; Deshmukh, R.; Zeng, Y.; Wilks, A.; Bunce, R. A.; Rivera, M. *J. Am. Chem. Soc.* **2003**, *125*, 11842−11852) and proposed as a signature of the HO distal cavity. The conservation of slow labile proton exchange with solvent from pH 7.0 to 10.8 confirms the extraordinary dynamic stability of *Nm*HO complexes. Comparison of the diamagnetic contribution to the labile proton chemical shifts in the aquo and hydroxide complexes reveals strongly conserved bond strengths in the distal H-bond network, with the exception of the distal His53 $N_{\epsilon 1}H$. The iron-ligated water is linked to His53 primarily by a pair of nonligated, ordered water molecules that transmit the conversion of the ligated H-bond donor (H_2O) to a H-bond acceptor (OH^-), thereby increasing the H-bond donor strength of the His53 side chain.

Introduction

Heme oxygenase (HO) is a nonmetal enzyme that uses protohemin (PH) as both a cofactor and substrate to generate biliverdin, iron, and CO.[1−6] HOs are widely distributed. In mammals, they maintain iron homeostasis,[7] produce the precursor to the powerful antioxidant[4,8] biliverdin, and generate CO as a potential neural messenger.[8,9] In plants and cyanobacteria, HOs generate the linear tetrapyrroles as precursors to light-harvesting pigments.[10] The HOs identified for a number of pathogeneic bacteria[11−13] appear to have as their major role the "mining" of iron to infect a host.[3,5] Two such HOs of interest here are *Neisseria meningitidis*, *Nm*HO (also called HemO[12,14,15]) and *Pseudomonas aeruginosa*, *Pa*HO.[13,16,17] A common mechanism, worked out on the mammalian HOs, appears operative in the various HOs.[2−4,18] The resting-state substrate complex, HO−PH−H_2O, is first reduced, after which O_2 is ligated.[19] Upon adding another electron and a proton, the ferric hydroperoxy species (Figure 1A) is formed,[20−22] which attacks one of the *meso*-carbons to yield the initial *meso*-hydroxy-PH inter-

[†] University of California.
[‡] Yamagata University School of Medicine.

(1) Tenhunen, R.; Marver, H. S.; Schmid, R. *J. Biol. Chem.* **1969**, *244*, 6388−6394.
(2) Yoshida, T.; Migita, C. T. *J. Inorg. Biochem.* **2000**, *82*, 33−41.
(3) Wilks, A. *Antioxid. Redox Signaling* **2002**, *4*, 603−614.
(4) Ortiz de Montellano, P. R.; Auclair, K. In *The Porphyrin Handbook*; Kadish, K. M., Smith, K. M., Guilard, R., Eds.; Elsevier Science: San Diego, CA, 2003; Vol. 12, 175−202.
(5) Frankenberg-Dinkel, N. *Antioxid. Redox Signaling* **2004**, *6*, 825−834.
(6) Rivera, M.; Zeng, Y. *J. Inorg. Biochem.* **2005**, *99*, 337−354.
(7) Uzel, C.; Conrad, M. E. *Semin. Hematol.* **1998**, *35*, 27−34.
(8) Maines, M. D. *Annu. Rev. Pharmacol. Toxicol.* **1997**, *37*, 517−554.
(9) Verma, A.; Hirsch, D. J.; Glatt, C. E.; Ronnett, G. V.; Snyder, S. H. *Science* **1993**, *259*, 381−384.
(10) Beale, S. I. *Ciba Found. Symp.* **1994**, *180*, 156−168.
(11) Wilks, A.; Schmitt, M. P. *J. Biol. Chem.* **1998**, *273*, 837−841.
(12) Zhu, W.; Willks, A.; Stojiljkovic, I. *J. Bacteriol.* **2000**, *182*, 6783−6790.
(13) Ratliff, M.; Zhu, M.; Deshmukh, R.; Wilks, A.; Stojiljkovic, I. *J. Bacteriol.* **2001**, *183*, 6394−6403.
(14) Schuller, D. J.; Zhu, W.; Stojiljkovic, I.; Wilks, A.; Poulos, T. L. *Biochemistry* **2001**, *40*, 11552−11558.
(15) Friedman, J. M.; Lad, L.; Deshmukh, R.; Li, H. Y.; Wilks, A.; Poulos, T. L. *J. Biol. Chem.* **2003**, *278*, 34654−34659.
(16) Caignan, G. A.; Deshmukh, R.; Wilks, A.; Zeng, Y.; Huang, H.-W.; Moenne-Loccoz, P.; Bunce, R. A.; Eastman, M. A.; Rivera, M. *J. Am. Chem. Soc.* **2002**, *124*, 14879−14892.
(17) Friedman, J.; Lad, L.; Li, H.; Wilks, A.; Poulos, T. L. *Biochemistry* **2004**, *43*, 5239−5245.
(18) Ortiz de Montellano, P. R.; Wilks, A. *Adv. Inorg. Chem.* **2001**, *51*, 359−407.
(19) Yoshida, T.; Noguchi, M.; Kikuchi, G. *J. Biol. Chem.* **1980**, *255*, 4418−4420.
(20) Wilks, A.; Torpey, J.; Ortiz de Montellano, P. R. *J. Biol. Chem.* **1994**, *269*, 29553−29556.
(21) Ortiz de Montellano, P. R. *Acct. Chem. Res.* **1998**, *31*, 543−549.
(22) Davydov, R. M.; Yoshida, T.; Ikeda-Saito, M.; Hoffman, B. M. *J. Am. Chem. Soc.* **1999**, *121*, 10656−10657.

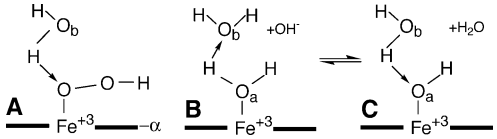

Figure 1. Geometry of a ferric porphyrin ligated: (A) hydroperoxide, (B) neutral water molecule *a*, and (C) hydroxide. The latter two species are at equilibrium at any solution pH value; this equilibrium shifts to the right with increasing pH. Nonligated water molecule *b* in the distal pocket provides the major interaction for the axially ligated water molecule[14] serving as an acceptor to molecule *a* in (B). Both (A) hydroperoxide and (C) hydroxide serve as acceptors to water *b*.

mediate. The hydroperoxy species as the hydroxylation agent in HO is in contrast to the active ferryl species in cytochromes P450 and peroxidases.[4,20] The structural basis for stabilizing the hydroperoxy species and destabilizing O−O bond cleavage is of considerable current interest.[22−24] Although mechanistic studies are consistent with electrophilic rather than nucleophilic attack on the meso carbon,[20] a free-radical contribution has not been ruled out.[6,25]

Due to the instability of the oxy and hydroperoxy species at ambient temperatures,[22−24,26] structural characterization by crystallography or ^{1}H NMR, with one exception,[26] has had to resort to model complexes, ferrous HO−PH−NO[15,27] and HO−PH−CO,[28] and ferric HO−PH−N_3 and HO−PH−CN[28] for X-ray crystallography and the ferric HO−PH−CN[16,29−34] (or HO−PH−N_3) complexes for NMR as models for ferrous HO−PH−O_2 complex. The diverse crystal structures of mammalian[27,28,35,36] and bacterial[14,15,17,26,37] HOs reveal a common fold where the placement of the distal helix close to the heme plane blocks three of the four meso positions from attack by Fe^{3+}−OOH, and steric interaction of the ligand directly with the distal helix backbone "orients/tilts" the axial ligand toward the fourth, unblocked meso position. The crystal structures, moreover, locate a set of three conserved, nonligated, ordered water molecules in the distal pocket that are implicated in stabilizing the Fe^{3+}−OOH species and likely serve as the proton conduit to the active site.[15,26,27,36] Solution ^{1}H NMR studies have shown[31−34] that HOs possess an extended H-bond network in the distal pocket with some stronger-than-usual H-bonds that serve as a scaffold for not only the three "catalytically" implicated waters, but also to numerous other ordered water molecules. Based on the sum rule for *g* values applied to the ENDOR-detected HO ferric hydroperoxy species[22] and comparison to structurally characterized model compounds,[38,39] it has been proposed that, due to the unusual distal H-bonding interaction,[6] the low-spin HO−PH−OOH complex exists in a "d_{xy}" ($d^2_{xz}d^2_{yz}d_{xy}$) rather than the more conventional "d_π" ($d^2_{xy}(d_{xz},d_{yz})^3$) orbital ground state, with the PH exhibiting significant ruffling.[38−40] This "ruffling" in the d_{xy} ground state could result in a large, unpaired spin density (observed by ^{13}C NMR) appearing at the *meso*-carbons. Such a d_{xy} ground state has been viewed as a unique self-activating role of PH in HOs.[6,40]

The reactive HO−PH−OOH species is sufficiently stable for spectroscopic study only at cryogenic temperatures.[22−24] However, solution ^{13}C NMR studies on *Pa*HO−PH−OH-containing, ^{13}C-labeled PH revealed[40] large *meso*-carbon spin densities indicative[38,39] of the d_{xy} orbital ground state, suggesting that the HO−PH−OH complex may serve as a valid model for the unusual distal H-bond interaction that stabilizes the d_{xy} ground state in *Pa*HO−PH−OOH. Confirming the d_{xy} ground state by ^{13}C NMR, however, requires selective ^{13}C labeling that is readily achievable for PH[40] but would require total synthesis for modified substrates whose altered basicity would modulate[41−44] the axial ligand H-bonding interaction between the distal water molecules and H-bonding network. The d_{xy} ground state, however, possesses additional magnetic resonance signatures that have more general applicability to diverse HO complexes. Thus the d_π and d_{xy} orbital ground states differ characteristically[38,39,45,46] in the *sign of their axial anisotropy*, $\Delta\chi_{ax}$. Although low-spin iron(III) in either orbital state exhibits a rhombic χ tensor (or *g* tensor), the axial $\Delta\chi_{ax}$ is always much larger than $\Delta\chi_{rh}$ by factors of ~3 and dominates the dipolar field of the iron. The determination of the sign of the axial anisotropy could be most directly determined by EPR, but would require single crystals that should allow detection at ambient temperatures. The former is difficult and the latter is not possible because of the rapid electron spin relaxation at all but cryogenic temperatures. However, the sign (and magnitude) of anisotropy of χ can be directly determined by solution ^{1}H NMR using experimental dipolar shifts, δ_{dip}, induced in the protein matrix by the anisotropic χ tensor. This shift is given by:[47−49]

$$\delta_{dip} = (24\pi N_A)^{-1}[2\Delta\chi_{ax}(3\cos^2\theta' - 1)R^{-3} + 3\Delta\chi_{rh}(\sin^2\theta'\cos 2\Omega)R^{-3}]\Gamma(\alpha,\beta,\gamma) \quad (1)$$

where x', y', z' (R, θ', Ω') are proton positions in an arbitrary,

(23) Davydov, R.; Kofman, V.; Fujii, H.; Yoshida, T.; Ikeda-Saito, M.; Hoffman, B. M. *J. Am. Chem. Soc.* **2002**, *124*, 1798−1808.
(24) Davydov, R.; Chemerisov, S.; Werst, D. E.; Rajh, T.; Matsui, T.; Ikeda-Saito, M.; Hoffman, B. M. *J. Am. Chem. Soc.* **2004**, *126*, 15960−15961.
(25) Kamachi, T.; Shestakov, A. F.; Yoshizawa, K. *J. Am. Chem. Soc.* **2004**, *126*, 3672−3673.
(26) Unno, M.; Matsui, T.; Chu, G. C.; Coutoure, M.; Yoshida, T.; Rousseau, D. L.; Olson, J. S.; Ikeda-Saito, M. *J. Biol. Chem.* **2004**, *279*, 21055−21061.
(27) Lad, L.; Wang, J.; Li, H.; Friedman, J.; Bhaskar, B.; Ortiz de Montellano, P. R.; Poulos, T. L. *J. Mol. Biol.* **2003**, *330*, 527−538.
(28) Sugishima, M.; Sakamoto, H.; Noguchi, M.; Fukuyama, K. *Biochemistry* **2003**, *42*, 9898−9905.
(29) Gorst, C. M.; Wilks, A.; Yeh, D. C.; Ortiz de Montellano, P. R.; La Mar, G. N. *J. Am. Chem. Soc.* **1998**, *120*, 8875−8884.
(30) La Mar, G. N.; Asokan, A.; Espiritu, B.; Yeh, D. C.; Auclair, K.; Ortiz de Montellano, P. R. *J. Biol. Chem.* **2001**, *276*, 15676−15687.
(31) Li, Y.; Syvitski, R. T.; Auclair, K.; Wilks, A.; Ortiz de Montellano, P. R.; La Mar, G. N. *J. Biol. Chem.* **2002**, *277*, 33018−33031.
(32) Li, Y.; Syvitski, R. T.; Auclair, K.; Ortiz de Montellano, P. R.; La Mar, G. N. *J. Am. Chem. Soc.* **2003**, *125*, 13392−13403.
(33) Li, Y.; Syvitski, R. T.; Chu, G. C.; Ikeda-Saito, M.; La Mar, G. N. *J. Biol. Chem.* **2003**, *279*, 6651−6663.
(34) Liu, Y.; Zhang, X.; Yoshida, T.; La Mar, G. N. *Biochemistry* **2004**, *43*, 10112−10126.
(35) Schuller, D. J.; Wilks, A.; Ortiz de Montellano, P. R.; Poulos, T. L. *Nature Struct. Biol.* **1999**, *6*, 860−867.
(36) Sugishima, M.; Sakamoto, H.; Higashimoto, Y.; Omata, Y.; Hayashi, S.; Noguchi, M.; Fukuyama, K. *J. Biol. Chem.* **2002**, 45086−45090.
(37) Hirotsu, S.; Chu, G. C.; Unno, M.; Lee, D.-S.; Yoshida, T.; Park, S.-Y.; Shiro, Y.; Ikeda-Saito, M. *J. Biol. Chem.* **2004**, *279*, 11937−11947.
(38) Walker, F. A. In *The Porphyrin Handbook*; Kadish, K. M., Smith, K. M., Guilard, R., Eds.; Academic Press: Boston, 2000; Vol. 5, 1−183.
(39) Rivera, M.; Caignan, G. A.; Astashkin, A. V.; Raitsimring, A. M.; Shokhireva, T. K.; Walker, F. A. *J. Am. Chem. Soc.* **2002**, *124*, 6077−6089.
(40) Caignan, G. A.; Deshmukh, R.; Zeng, Y.; Wilks, A.; Bunce, R. A.; Rivera, M. *J. Am. Chem. Soc.* **2003**, *125*, 11842−11852.
(41) Caughey, W. S. In *Hemes and Hemoproteins*; Chance, B., Estabrook, R. W., Yonetani, T., Eds.; Academic Press: New York, 1966; 276−277.
(42) Brunori, M.; Amiconi, G.; Antonini, E.; Wyman, J.; Zito, R.; Rossi-Fanolli, A. *Biochim. Biophys. Acta* **1968**, *154*, 315−322.
(43) Cowgill, R. W.; Clark, W. M. *J. Biol. Chem.* **1952**, *198*, 33−61.
(44) McGrath, T. M.; La Mar, G. N. *Biochim. Biophys. Acta* **1978**, *534*, 99−111.
(45) Palmer, G. In *The Porphyrins*; Dolphin, D., Ed.; Academic Press: New York, 1979; Vol. IV, 313−353.
(46) Walker, F. A.; Simonis, U. *Biol. Magn. Reson.* **1993**, 12.

iron-centered coordinate system, $\Delta\chi_{ax}$ and $\Delta\chi_{rh}$ are the axial ($\chi_{zz} - 1/2(\chi_{xx} + \chi_{yy})$) and rhombic ($\chi_{xx} - \chi_{yy}$) anisotropies, and $\Gamma(\alpha, \beta, \gamma)$ is the Euler rotation that converts the reference coordinates, x', y', z', into the magnetic coordinate system, x, y, z, where χ is diagonal. The anisotropies and orientation of χ can be determined experimentally if sufficient experimental dipolar shifts can be assigned and valid crystal coordinates are available to generate x', y', z'. The anisotropy and orientation of numerous low-spin ferrihemoproteins in the conventional $S = {}^1/_2$, d_π ground state have been determined, and they have the common property[38,49] of large positive $\Delta\chi_{ax} > 2 \times 10^{-8}$ m^3/mol and much smaller rhombic anisotropies with $|\Delta\chi_{ax}/\Delta\chi_{rh}| \approx 3-4$.

We have been engaged in a study of the functionally relevant molecular and electronic structural-information content of the NMR spectra for a range of paramagnetic substrate complexes of both mammalian[30−32] and bacterial[33,34,50] HOs. A particularly attractive candidate is the HO from the pathogeneic bacterium *Neisseriae meningitidis*, *Nm*HO, a ~210 residue enzyme.[3,12] The distal ligand in the *Nm*HO complex interacts with the distal water molecules[14,15] that, in turn, interact with a series of amino acid residues, either as acceptor or donors. *Nm*HO has the desirable properties of populating essentially a single PH orientation about the α-,γ-meso axis, which is the same in both solution[6,34,50] and crystals[14,15] and which displays superior resolution that has allowed ^{1}H NMR characterization of a significant fraction of the complex in both the low-spin,[34] *Nm*HO−PH−CN, and the high-spin,[50] *Nm*HO−PH−H_2O, complexes. ^{1}H NMR spectra of only one hydroxide HO complex, *Pa*HO−PH−OH, have been reported[40] for which the heme signals were assigned by ^{13}C labeling. No information was provided on the protein matrix that could shed light on the sign or magnitude of the magnetic anisotropy.

We report here on the thermodynamics and dynamics of the *Nm*HO−PH−H_2O ⇔ *Nm*HO−PH−OH interconversion and provide the characterization of the electronic/magnetic properties of the latter complex. The results indicate that *Nm*HO−PH−OH possesses large positive axial anisotropy that dictates it exists in the d_π ground state. In addition to characterizing the electronic/magnetic properties of the *Nm*HO−PH−OH complex, we investigate the manner in which the H-bond donor in the distal pocket responds to conversion of the axial H-bond donor, ligated water (water *a* in Figure 1B) to a nonligated water *b*, to an axial H-bond acceptor OH^- that serves as a H-bond acceptor to water *b*.

Experimental Section

Sample Preparation. The apo-*Nm*HO samples used in this study are the same as described in detail previously.[34] Stoichiometric amounts of protohemin, PH (Figure 2), dissolved in 0.1 M KOH in ^1H_2O were added to apo-*Nm*HO in phosphate buffer (50 mM, pH 7.0). The substrate complex was purified by column chromatography on Sephadex G25 and yielded samples ~3 mM in *Nm*HO−PH−H_2O at pH 7.0. Samples in ^1H_2O were converted to ^2H_2O by column chromatography.[51] Sample pH for reference spectra in the range 7.0−10.8 was altered by adding incremental 0.1 M KO^{2}H in ^2H_2O solution to *Nm*HO−PH−^2H_2O in ^2H_2O, 50 mM phosphate at 25 °C. For long-term (> ~24 h) 2D NMR spectra, samples were buffered at the desired pH with phosphate (pH 7.0−8.7) or bicarbonate (pH 9.1−10.8). The pH values in ^2H_2O are uncorrected for isotope effects.

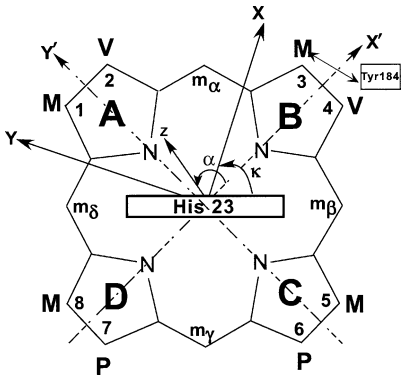

Figure 2. Schematic structure of the heme pocket of *Nm*HO−PH−H_2O, viewed from the proximal side, showing the numbering of the protoheme (PH) skeleton, the orientation of the axial His23 imidazole plane, and the position of Tyr184 relative to pyrrole B. Also shown is the arbitrary, iron-centered reference coordinate system, x', y', z', where x' and y' are in the heme plane passing through pyrroles N_B and N_A, respectively, and z' points to the proximal side. The magnetic coordinate system, x, y, z, for an axially anisotropic paramagnetic susceptibility tensor, χ, where χ is diagonal, is defined by a tilt from the unique or z axis from the heme normal (z' axis) by an angle β (not shown) and in a direction defined by the angle α between the projection of z on the x', y' plane, and the x' axis.

NMR Spectroscopy. ^{1}H NMR data were collected on Bruker AVANCE 500 and 600 spectrometers operating at 500 and 600 MHz, respectively. Reference spectra were collected in ^2H_2O over the temperature range 15−35 °C at both a repetition rate of 1 s^{-1} over 40 ppm spectral width and at 5 s^{-1} over a 200 ppm bandwidth. Steady-state, magnetization-transfer (NOE or exchange) difference spectra were generated from spectra with on-resonance and off-resonance saturation of the desired signals; to detect exchange with H_2O, selective 3:9:19 excitation was used.[52] Chemical shifts are referenced to 2,2-dimethyl-2-silapentane-5-sulfonate (DSS) through the water resonance, calibrated at each temperature. Nonselective T_1s were determined by the standard inversion−recovery pulse sequence and estimated from the null point. 600 MHz NOESY[53] (two-dimensional nuclear Overhauser spectroscopy) spectra (mixing time 40 ms; repetition rate 2 s^{-1}) and 500 MHz clean-TOCSY (two-dimensional total correlation spectroscopy) (to suppress ROESY response[54]) spectra (25°, 35 °C, spin lock 25 ms) using MLEV-17[55] were recorded over a bandwidth of 25 kHz (NOESY) and 12 kHz (TOCSY) with recycle times of 500 ms and 1s, using 512 t1 blocks of 128 and 256 scans each consisting of 2048 t2 points. Two-dimensional (2D) data sets were processed using Bruker XWIN software on a Silicon Graphics Indigo workstation. The processing consisted of 30°- or 45°-sine-squared-bell-apodization in both dimensions, and zero-filling to 2048 × 2048 data points prior to Fourier transformation.

Magnetic Axes Determination. The location of the magnetic axes was determined by finding the Euler rotation angles, $\Gamma(\alpha,\beta,\gamma)$, that rotate the crystal-structure-based, iron-centered reference coordinate system, x', y', z', into the magnetic coordinate system, x, y, z, where the paramagnetic susceptibility tensor, χ, is diagonal and where α, β, γ are the three Euler angles.[34,47−50] The angle β dictates the tilt of the major magnetic axis, z, from the heme normal z', α reflects the direction

(47) Williams, G.; Clayden, N. J.; Moore, G. R.; Williams, R. J. P. *J. Mol. Biol.* **1985**, *183*, 447−460.
(48) Emerson, S. D.; La Mar, G. N. *Biochemistry* **1990**, *29*, 1556−1566.
(49) La Mar, G. N.; Satterlee, J. D.; de Ropp, J. S. In *The Porphyrins Handbook*; Kadish, K. M., Smith, K. M., Guilard, R., Eds.; Academic Press: San Diego, 2000; Vol. 5, 185−298.
(50) Liu, Y.; Zhang, X.; Yoshida, T.; La Mar, G. N. *J. Am. Chem. Soc.* **2005**, *127*, 6409−6422.
(51) Johnston, P. D.; Figueroa, N.; Redfield, A. G. *Proc. Natl. Acad. Sci. U.S.A.* **1979**, *76*, 3130−3134.
(52) Piotto, M.; Sandek, V.; Sklenar, V. *J. Biomol. NMR* **1992**, *2*, 661−666.
(53) Jeener, J.; Meier, B. H.; Bachmann, P.; Ernst, R. R. *J. Chem. Phys.* **1979**, *71*, 4546−4553.
(54) Griesinger, C.; Otting, G.; Wüthrich, K.; Ernst, R. R. *J. Am. Chem. Soc.* **1988**, *110*, 7870−7872.
(55) Bax, A.; Davis, D. G. *J. Magn. Reson.* **1985**, *65*, 355−360.

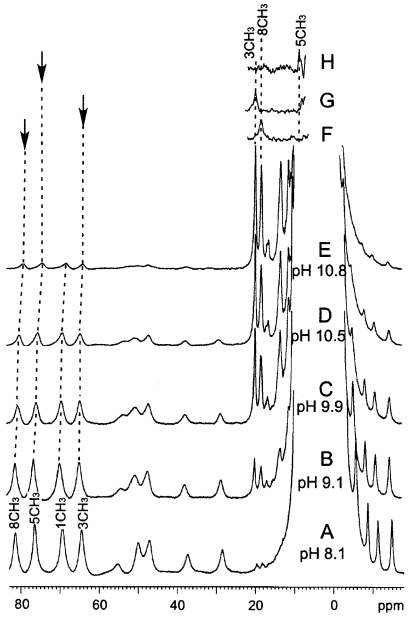

Figure 3. Resolved portions of the 500 MHz ^{1}H NMR spectrum of *Nm*HO−PH−H_2O/OH at 25 °C as a function of solution pH. The predominant *Nm*HO−PH−H_2O complex with its assigned signals is shown at (A) pH 8.1, (B) pH 9.1, (C) pH 9.9, (D) pH 10.5 (6:94% *Nm*HO−PH−H_2O/*Nm*HO−PH−OH), and (E) pH 10.8. The magnetization-transfer difference spectra for *Nm*HO−PH−OH upon saturating the assigned *Nm*HO−PH−H_2O heme methyl[50] (as indicated by vertical arrow) are shown for the (F) 8-CH_3, (G) 3-CH_3, and (H) 5-CH_3.

of this tilt and is defined as the angle between the projection of the z axis on the heme plane and the x' axis (Figure 2), and $\kappa \approx (\alpha + \gamma)$ is the angle between the projection of the x, y axes onto the heme plane and locates the rhombic axes (Figure 2). In the present case, we consider the tensor to be axially symmetric, so that $\Delta\chi_{rh} = 0$, and γ becomes irrelevant. The magnetic axes were determined by a least-squares search for the minimum in the error function, F/n:[34,47−50]

$$F/n = \sum_{i=1}^{n} |\delta_{dip}(\text{obs}) - \delta_{dip}(\text{calc})|^2 \qquad (2)$$

with observed dipolar shift, δ_{dip}(obs) given by:

$$\delta_{dip}(\text{obs}) = \delta_{DSS}(\text{obs}) - \delta_{DSS}(\text{dia}) \qquad (3)$$

where δ_{DSS}(obs) and δ_{DSS}(dia) are the chemical shifts, in ppm, referenced to DSS, for the paramagnetic *Nm*HO−PH−OH complex and an isostructural diamagnetic complex, respectively. In the absence of an experimental δ_{DSS}(dia) for the latter, it may be reasonably estimated[56,57] from the available molecular structure[14] and available computer programs,[56,57] as described previously for *Nm*HO−PH−CN[34] and *Nm*HO−PH−H_2O.[50]

Results

pH Titration. The influence of solution pH on the resolved portions of the 500 MHz ^{1}H NMR spectra of *Nm*HO−PH−H_2O in ^2H_2O in the pH range 8.0−10.8 is illustrated in Figure 3. The loss of intensity in Figure 3A−E, without concomitant line-broadening, of the assigned[50] heme methyl peaks in the 60−85 ppm window for high-spin *Nm*HO−PH−H_2O and the appearance of two resolved, apparent heme methyl peaks in the 18−20 ppm window, typical for the expected low-spin *Nm*HO−PH−OH complex,[49] dictate that the deprotonation/protonation of the exogenous ligand is slow on the NMR time scale.[58] In concert with this observation, all signals, including ones for inconsequentially relaxed protons and with only 0.1 ppm shift difference in the two species, similarly exhibited slow exchange, indicating the exchange rate is $<10^3$ s^{-1}. The sum of the intensities of an assigned [50] low-field heme methyl peak of *Nm*HO−PH−H_2O and that of the proposed (see below) heme methyl peak of *Nm*HO−PH−OH in the pH titration in ^2H_2O remained constant relative to the intensity of the diamagnetic envelope, within the experimental uncertainty of ∼15%. This dictates that only two species are detectably populated and leads to the Henderson−Hasselbalch plot in Figure 4 (○). The data at the strongly alkaline pH are likely suspect due to generation of a detectable third species above pH 10.2. However, the integration of the spectra in Figure 4 in the pH range 9.1−10.5 allows the estimate of the pK as 9.8 in ^2H_2O. The single spectrum at pH 10.2 in ^1H_2O, results in the filled marker in Figure 4 and indicates that the pK in ^1H_2O is ∼0.4 units lower on the pH scale, or pK(^1H_2O) ≈ 9.4.

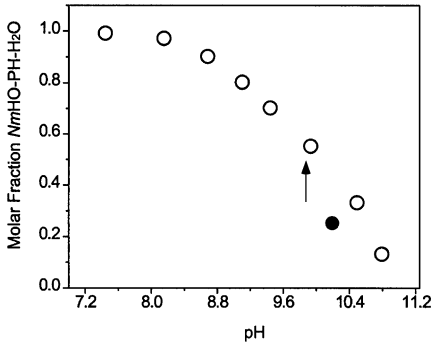

Figure 4. A Henderson−Hasselbalch plot (mole fraction *Nm*HO−PH−OH in *Nm*HO−PH−H_2O/*Nm*HO−PH−OH mixtures as a function of pH) in ^2H_2O solution, at 25 °C, as determined from the relative intensities of the heme 3-CH_3 signal in the two complexes. Data in ^2H_2O are shown as open circles. The estimated pK ≈ 9.8 in ^2H_2O is shown by a vertical arrow. The single data point recorded in ^1H_2O solution at pH 10.2 is shown as a closed circle.

The dominant *Nm*HO−PH−OH complex at pH 10.5 and 10.8 exhibited T_1s ≈ 8−9 ms for the two resolved low-field heme methyl peaks and T_1s ≈ 7−10 ms for the apparent composite peak centered near 15 ppm (data not shown), which is assumed to arise from α-protons from the propionates and vinyl groups. At these alkaline pH values, exchange-transfer contributes negligibly to the effective T_1s, dictating that they are the true T_1s in the hydroxide complex. The upfield shoulder of the *Nm*HO−PH−OH spectrum at pH 10.5 exhibits one rapidly relaxed single proton peak with T_1s ≈ 12 ms (not shown, see Supporting Information) that has no detectable NOESY cross-peak. The upfield resonance position and relaxation rate are consistent with expectations for a vinyl H_β.[49]

Heme Methyl Assignments for *Nm*HO−PH−OH. Saturation of the assigned low-field methyl peaks[50] for the high-spin *Nm*HO−PH−H_2O complex in ^2H_2O at pH 8.9 results in the saturation-transfer-difference[58] spectra illustrated in Figure 3F−H. These lead to the unambiguous assignment of the resolved 8CH_3 (Figure 3F) and 3CH_3 (Figure 3G) signals of *Nm*HO−PH−OH and locate the 5CH_3 signal (Figure 3H) at the low-

(56) Neal, S.; Nip, A. M.; Zhang, H.; Wishart, D. S. *J. Biomol. NMR* **2003**, *26*, 215−240.
(57) Cross, K. J.; Wright, P. E. *J. Magn. Reson.* **1985**, *64*, 220−231.
(58) Sandström, J. *Dynamic NMR Spectroscopy*; Academic Press: New York, 1982.

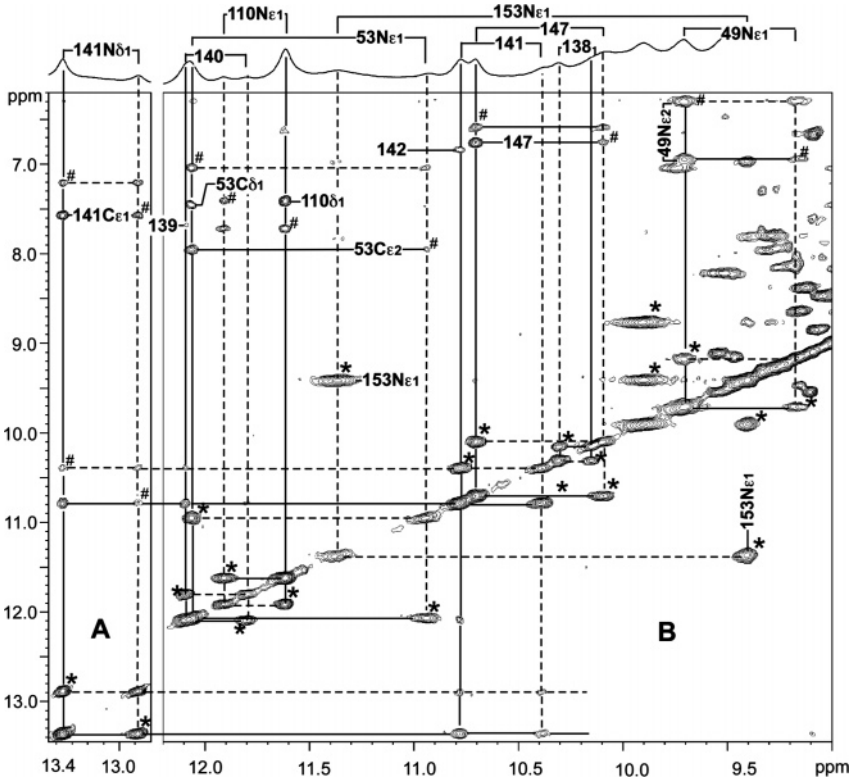

Figure 5. Low-field resolved portion of the 600 MHz ^{1}H NMR reference spectrum of ~25% *Nm*HO−PH−H_2O; ~75% *Nm*HO−PH−OH in ^1H_2O at pH 10.2 and 25 °C with bars to connect the position of the two exchanging peaks, as previously assigned for the *Nm*HO−PH−H_2O complex. (A, B) Pertinent portion of the 600 MHz NOESY/EXSY spectrum (mixing time 40 ms, repetition rate 2 s^{-1}) illustrating the NOESY, exchange (EXSY; peaks marked by *), and exchange-transferred NOESY peaks (marked by #) among the low-field labile protons. The unambiguous assignment of the labeled peaks for *Nm*HO−PH−OH is completely dependent on the previous unambiguous assignments carried out on essentially pure *Nm*HO−PH−H_2O.[50] Again, protons in *Nm*HO−PH−H_2O are shown by dashed lines, whereas those in *Nm*HO−PH−OH are shown by solid lines. Signals are identified by residue number and position, except peptide NHs, which are labeled solely by residue number.

field edge of the aromatic envelope. Saturation of the $1CH_3$ peak in *Nm*HO−PH−H_2O failed to reveal any clear signal attributable to $1CH_3$ in *Nm*HO−PH−H_2O, and it is likely under the weak off-resonance saturation of the diamagnetic envelope resulting from the strong saturation field necessary to saturate the high-spin complex peak. Hence, we conclude that $1CH_3$ is located within the 1−7 ppm window.

The effect of temperature (not shown, see Supporting Information) on the chemical shifts for the resolved *Nm*HO−PH−OH methyl peak reveals weak Curie behavior for $3CH_3$ peak (apparent intercept at $T^{-1} = 0$ of 19 ppm), and weak anti-Curie behavior for the $8CH_3$ peak (apparent intercept at $T^{-1} = 0$ of 30 ppm).

Residue Assignment Protocols. All 2D spectra (both NOESY and TOCSY) with more than ~10% *Nm*HO−PH−OH present (above pH 8.5) exhibited cross-peaks that were strongly dominated by chemical exchange between *Nm*HO−PH−H_2O and *Nm*HO−PH−OH. This strong dominance of exchange cross-peaks is obvious for resolved resonances where such cross-peaks are instantly recognizable, as illustrated for the low-field spectral window in Figure 5. Brackets above the reference trace over the 2D map in Figure 5 connect the two sets of resonances (relative intensities ≈ 3:1) for *Nm*HO−PH−OH and *Nm*HO−PH−H_2O, where the resonances of the latter complex have been assigned previously.[50] In Figure 5, as in the following Figures 6−8, direct exchange cross-peaks are labeled by asterisks (*), with the *Nm*HO−PH−OH and *Nm*HO−PH−H_2O frequencies marked by solid and dashed lines, respectively. Peaks are labeled by residue number and position, except for peptide NHs, which are labeled solely by residue number. Exchange-transferred NOESY cross-peaks (i.e., an NOE to a *Nm*HO−PH−H_2O proton *i*, that it is transferred to the same proton, *i*, in the *Nm*HO−PH−OH complex), are labeled by the pound marker (#). The NOESY spectrum in Figure 5 is dominated not only by direct-exchange cross-peaks (marked *), but also by exchange-transferred NOESY cross-peaks (marked #) in ^1H_2O solution. For example, the *Nm*HO−PH−OH His141 $N_{\delta 1}H$ signal at 13.35 ppm (solid lines in Figure 5A) exhibits a *direct exchange cross-peak* not only to the $N_{\delta 1}H$ in the *Nm*HO−PH−H_2O complex at ~12.9 ppm but also to the 141NH of *Nm*HO−PH−H_2O (marked by #) at 10.4 ppm.

Figure 6A−C presents the reference spectra and the pertinent portions of the NOESY spectra for the upfield resolved spectral window as a function of increasing pH. Even at pH 7.2 (~3% *Nm*HO−PH−OH), exchange cross-peaks can be detected (Figure 6A′), whereas at pH 8.7 (~12% *Nm*HO−PH−OH), exchange cross-peaks are as intense as any intramolecular NOESY cross-peaks (Figure 6B′). At pH 10.2 (~75−80% *Nm*HO−PH−OH; see Figure 6C′), by far the strongest cross-peaks still originate from exchange. Thus, with significant population of both isomers, a typical 2D map was dominated by exchange cross-peaks that strongly obscure intramolecular NOESY cross-peaks. It was not possible to identify a set of conditions (pH, temperature, mixing time), which provided a map that is dominated by the desired intramolecular cross-peaks for the *Nm*HO−PH−OH complex.

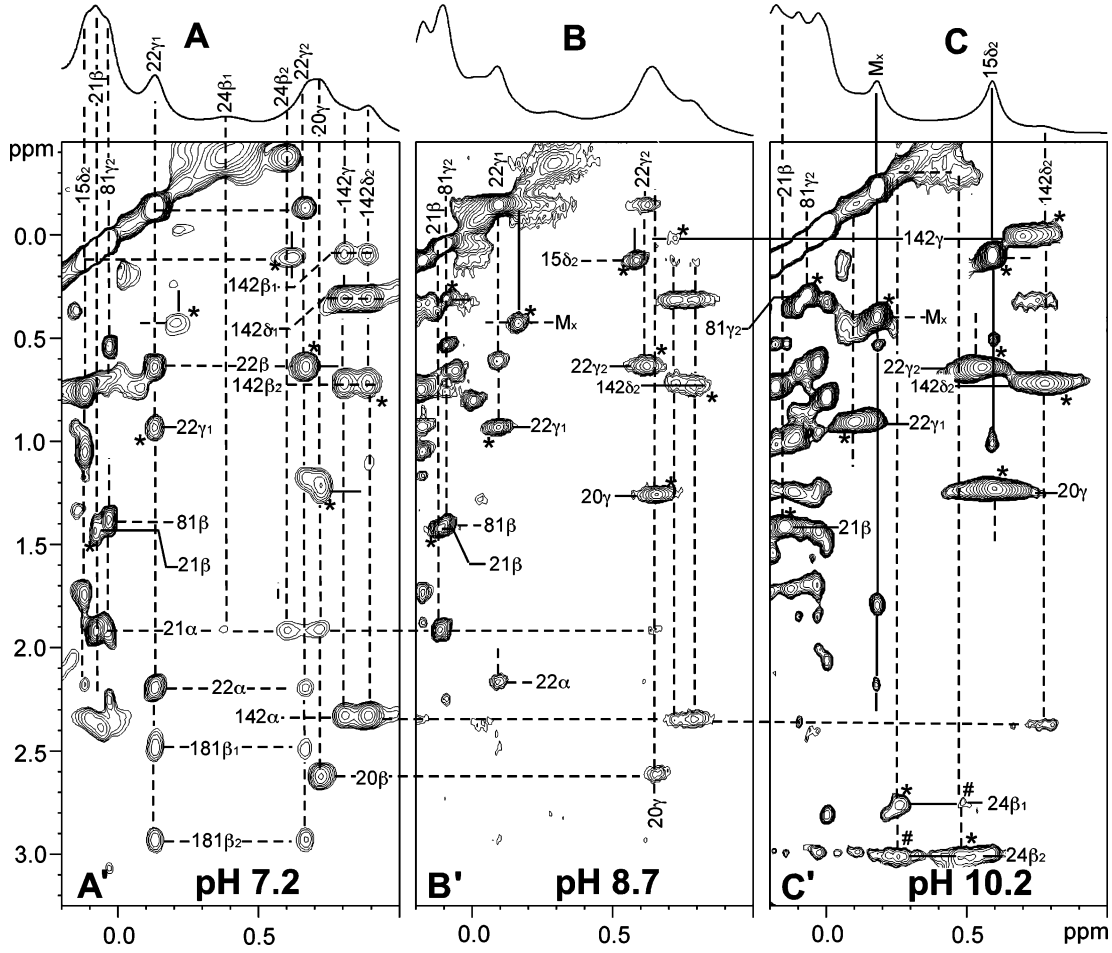

Figure 6. Resolved upfield portion of the 600 MHz ^{1}H NMR spectrum of *Nm*HO−PH−H_2O/OH in ^2H_2O at 25 °C at (A) pH 7.2, (B) pH 8.7, and (C) pH 10.2, illustrating the conversion of primarily *Nm*HO−PH−H_2O in A to primarily *Nm*HO−PH−OH in C. The pertinent portions of the 600 MHz ^{1}H NMR NOESY(EXSY) spectra (mixing time 40 ms, repetition rate 2 s^{-1}) are shown in A′, B′, C′ at the pH values corresponding to the reference spectra in A, B, C, respectively. Proton frequencies are labeled by residue number and position; peptide NHs are labeled solely by number. Dashed lines identify protons in *Nm*HO−PH−H_2O assigned previously, while solid lines identify newly assigned protons in *Nm*HO−PH−OH. Asterisks identify exchange peaks, and # identify exchange-transferred NOEs. Note weak exchange peaks Leu15 $C_{\delta 2}H_3$, and M_X (unassigned methyls) even at pH 7.2 (A′), which become stronger at both pH 8.7 (B′) and 10.2 (C′). Also note the diminishing intensity of intramolecular NOESY cross-peaks within *Nm*HO−PH−H_2O, and the increasing intensity of exchange cross-peak between *Nm*HO−PH−H_2O and *Nm*HO−PH−OH with increasing pH.

However, the above results suggest an approach where we inspect 2D maps as a function of pH, in which the appearance of new cross-peaks with increasing pH can be uniquely attributed to exchange peaks to the same proton in the *Nm*HO−PH−OH complex.

Low-Field Resolved Resonances in the H-Bond Network. Because the *Nm*HO−PH−H_2O cross-peaks have been uniquely assigned[50] in *Nm*HO−PH−H_2O at a sufficiently low pH that exchange cross-peak intensity is negligible, the identical assignments are trivially achieved for *Nm*HO−PH−OH complex, as shown in Figure 5. It is noted that, although most backbone NHs exhibit small to modest chemical-shift differences between the two complexes, those of several side chains, particularly His53 $N_{\epsilon 1}H$ and Trp153 $N_{\epsilon}H$, exhibit substantial chemical-shift differences. The chemical shifts for labile protons in *Nm*HO−PH−OH are listed in Table 1, where they can be compared to the previously reported[34] values for *Nm*HO−PH−H_2O.

High-Field Resolved Hyperfine Shifted Residues. The upfield portion of the NOESY spectrum with increasing pH (Figure 6) clearly leads to the assignment in *Nm*HO−PH−OH of each of the resolved upfield signals that had been previously assigned[50] in *Nm*HO−PH−H_2O. It is noted that in some cases, the exchange peak (marked by *) partially overlaps an intramolecular NOESY cross-peak for *Nm*HO−PH−H_2O (i.e., Val22 $\gamma 2/\beta$ NOESY cross-peak (Figure 6A′) and Val22 $\gamma 2$ exchange cross-peaks to *Nm*HO−PH−OH (Figures 6B′, 6C′)). Moreover, the appearance of a very weak cross-peak at pH 7.2 (Figure 6A), which increase strongly at higher pH (Figures 6B′, and 6C′), allows the connection between the two complexes of the two resolved methyls in the *Nm*HO−PH−OH complex (Leu15 $C_{\delta 2}H_3$ and M_X), with an unassigned methyl peak (designated M_X) at −0.22 ppm in *Nm*HO−PH−OH, but 0.37 ppm in *Nm*HO−PH−H_2O. Becakuse M_X in *Nm*HO−PH−OH exhibits insignificant hyperfine shifts (negligible temperature dependence), its assignment was not pursued further. The chemical shifts for residues with significant dipolar shifts (> |0.25| ppm) in *Nm*HO−PH−OH are listed in Table 2, and the data for the remaining assigned residues are listed in the Supporting Information.

Nonresolved Hyperfine-Shifted Resonances. Increasing the pH toward the alkaline region in ^2H_2O results in the detection of new cross-peaks (due to exchange), and the intensity increases with pH for three key, dipolar-shifted, aromatic residues assigned[34] in *Nm*HO−PH−H_2O, as illustrated at pH 8.7 in

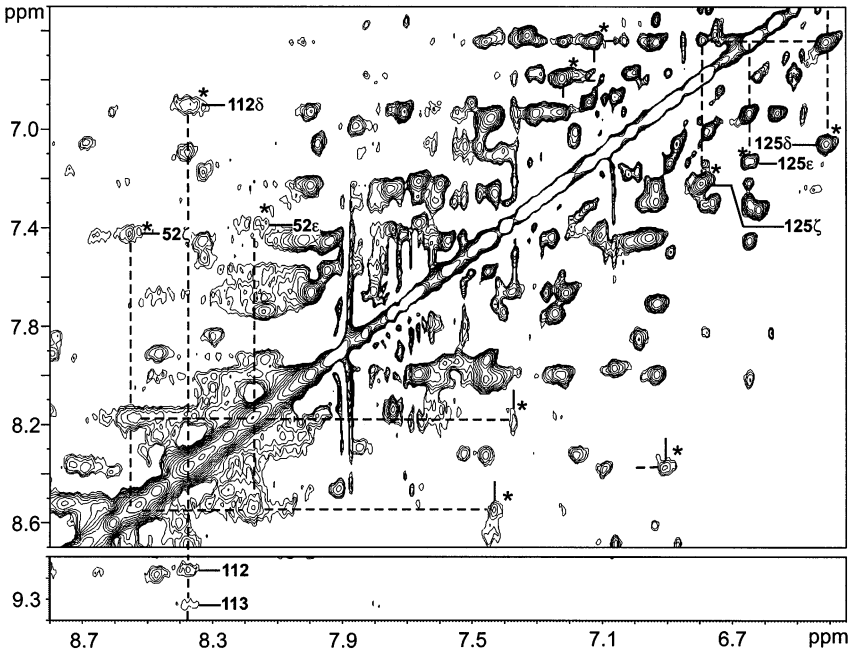

Figure 7. Aromatic proton portion of the 600 MHz ^{1}H NMR NOESY/EXSY spectrum (mixing time 40 ms; repetition rate 2 s^{-1}) for ~85% *Nm*HO−PH−H_2O and ~15% *Nm*HO−PH−OH at pH 8.7 in ^2H_2O solution, 50 mM in phosphate at 25 °C. New exchange peaks are marked by * for assigned aromatic rings in *Nm*HO−PH−H_2O and labeled for Phe52, Tyr112, and Phe125. Protons in *Nm*HO−PH−H_2O and *Nm*HO−PH−OH are shown by dashed and solid lines, respectively.

Figure 7. Exchange cross-peaks (marked *) from the well-resolved ring protons of Phe125 in *Nm*HO−PH−H_2O identify all of the protons in *Nm*HO−PH−OH. Similar cross-peaks are also observed for the C_ζH and C_ϵHs of Phe52 (marked by *); the C_δHs peak was found[34] to be very broad in *Nm*HO−PH−H_2O, which accounts for its undetectability in Figure 7. Last, an exchange cross-peak also identifies the Tyr112 C_δH cross-peak (marked by *). It is noteworthy that the various ring chemical shifts for each Phe52 and Phe125 in the *Nm*HO−PH−OH complex are sufficiently close to each other so as to preclude the resolution of the intraring NOESY cross-peaks in the pure *Nm*HO−PH−OH complex. The chemical shift for residues in *Nm*HO−PH−OH with significant dipolar shifts (> |0.25| ppm) are listed in Table 2, and the data for the remaining assigned residues are listed in the Supporting Information.

Tyr184 ring protons exhibited very broad signals whose NOESY cross-peak was marginally detectable in the *Nm*HO−PH−H_2O complex.[50] Its exchange cross-peaks to *Nm*HO−PH−OH are not detectable at pH 8.7, but at pH 10.5, where *Nm*HO−PH−OH with narrower lines is the dominant species, the ring exchange peaks are readily detected (Figure 8A). Seven assigned[50] slowly exchanging peptide NHs of *Nm*HO−PH−H_2O in ^2H_2O solution (residues 112−113, 182−184) also exhibit exchange peaks at pH 10.5 to their counterparts in *Nm*HO−PH−OH (Figure 8).

Dipolar Contacts within *Nm*HO−PH−OH. NOESY contacts among protons within the *Nm*HO−PH−OH complex are most readily identified for protons first identified by magnetization exchange from *Nm*HO−PH−H_2O. The sequential N_i−N_{i+1} contacts at pH 10.5 within the *Nm*HO−PH−OH complex for Tyr112-Glu115 and Ala182-Tyr184 are observed (Figure 8A) once the exchange cross-peaks between the H_2O and OH^- complexes are identified (Figure 7). Hence, these peptide NHs exhibit long $^1H \rightarrow {}^2H$ exchange lifetimes of over a period of several days even at pH 10.5. Also shown in Figure 8 are the exchange cross-peaks for the nearly degenerate His53 ring $C_{\delta 1}$H and $C_{\epsilon 2}$H (in *Nm*HO−PH−H_2O[50]) to their well-resolved positions in *Nm*HO−PH−OH (Figure 8A) and the exchange cross-peaks for the key His141 $C_{\delta 2}$H (Figure 8C).

The separate exchange cross-peaks for the Tyr184 ring (Figure 8A), when projected to the diagonal (Figure 8B), identify the intramolecular NOESY cross-peak for the Tyr184 ring within the *Nm*HO−PH−OH complex, as well as the expected intramolecular Tyr184 C_δHs to NH cross-peaks (Figure 8A). Saturation of the resolved $3CH_3$ peak of the *Nm*HO−PH−OH complex at pH 10.5 (Figure 8D) yields the NOE difference-spectrum with the expected cross-peaks to both ring protons of Tyr184, as well as to the C_δH of Phe52, whose exchange cross-peak with the same ring proton in *Nm*HO−PH−H_2O (marked*) is now also observed. The $3CH_3$ exhibited very similar NOE patterns in both *Nm*HO−PH−CN[34] and *Nm*HO−PH−H_2O.[50]

Anisotropy and Orientation of the Paramagnetic Susceptibility Tensor χ. The magnetic anisotropy of d_π, low-spin iron(III) is large, positive,[38,45,49] and primarily axial ($|\Delta\chi_{ax}/\Delta\chi_{rh}| \approx 3$), with $\Delta\chi_{ax} \approx 2.5 \times 10^{-8}$ m^3/mol. In contrast, the magnetic anisotropy of high-spin *Nm*HO−PH−H_2O is also largely axial[50] but negative with $\Delta\chi_{ax} \approx -2.0 \times 10^{-8}$ m^3/mol. In Table 2, we list the observed dipolar shift, δ_{dip}(obs), obtained via eq 1 for protons on residues with δ_{dip}(obs) > |0.25| ppm for *Nm*HO−PH−OH and compare these data with the previously reported data for the high-spin[50] *Nm*HO−PH−H_2O with negative $\Delta\chi_{ax}$ and low-spin[34] *Nm*HO−PH−CN with positive $\Delta\chi_{ax}$. It is apparent that in each case the *sign of the dipolar shift* in *Nm*HO−PH−OH is the same as that in *Nm*HO−PH−CN and opposite in sign to that in *Nm*HO−PH−H_2O, dictating that $\Delta\chi_{ax}$ is *positive* in *Nm*HO−PH−OH.

We first address the relative importance of the $\Delta\chi_{ax}$ and $\Delta\chi_{rh}$ term in describing the observed dipolar shift for *Nm*HO−PH−CN. The strong dominance of the axial anisotropy over the

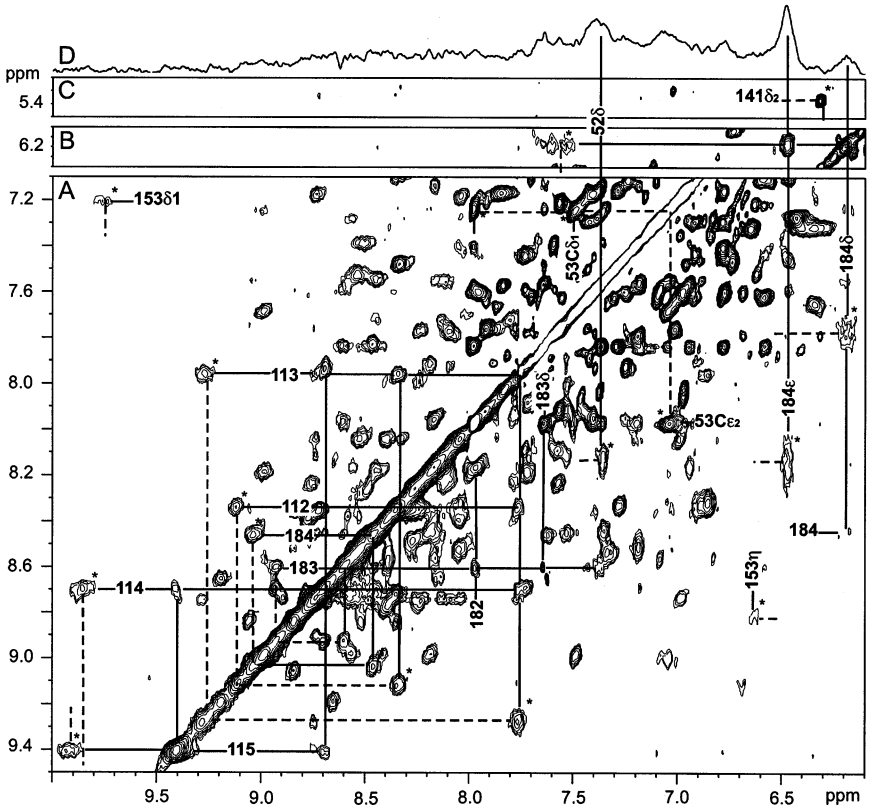

Figure 8. Low-field portion of the ^{1}H NMR NOESY/EXSY spectrum (mixing time 40 ms; repetition rate 2 s^{-1}) of ~20% *Nm*HO−PH−H_2O, ~80% *Nm*HO−PH−OH in ^2H_2O, 100 mM bicarbonate, at pH 10.5 and 25 °C illustrating exchange (EXSY) cross-peaks (marked by *) between *Nm*HO−PH−H_2O and *Nm*HO−PH−OH for slowly exchanging labile protons Tyr112-Glu115 and Ala182-Tyr184 (A), for the His53 ring $C_{\delta1}H$ and $C_{\epsilon2}H$ (A), Tyr184 ring proton (A), and His141 $C_{\delta2}H$ (C). The proton frequencies of *Nm*HO−PH−H_2O and *Nm*HO−PH−OH are marked by dashed and solid lines, respectively. Note that the sequential N_i-N_{i+1} cross-peaks within *Nm*HO−PH−OH are clearly observed for both helical fragments with slowly exchanging NHs. Panel (B) shows the intra-*Nm*HO−PH−OH Tyr184 ring, NOESY cross-peaks, and the expected Tyr184 C_δHs to peptide NH NOESY cross-peak (A). Panel (D) represents the steady-state 1D NOE difference spectrum within the *Nm*HO−PH−OH complex resulting upon saturating the 3-CH_3 of the *Nm*HO−PH−OH complex at 20 ppm, and yields the expected NOEs to the ring of Tyr184. The NOE to the Phe52 C_δH arises primarily from a very strong secondary NOE via the Tyr184 ring. Note that even at this extreme alkaline pH, EXSY cross-peaks are as intense as most NOESY cross-peaks.

observed dipolar shifts in *Nm*HO−PH−CN is evidenced by the fact that the change in $\Delta\chi_{ax}$ and its orientation are only weakly affected by setting $\Delta\chi_{rh} = 0$. Thus, a five-parameter search ($\Delta\chi_{ax}$, $\Delta\chi_{rh}$, α, β, and $\kappa = \alpha + \gamma$) (not shown; see Supporting Information) for *Nm*HO−PH−CN yields $\Delta\chi_{ax} = 2.48 \times 10^{-8}$ m^3/mol, $\Delta\chi_{rh} = -0.52 \times 10^{-8}$ m^3/mol, $\alpha = 280 \pm 10°$, $\beta = 8 \pm 1°$, $\kappa = 40 \pm 10°$. When $\Delta\chi_{rh}$ is set equal to zero for *Nm*HO−PH−CN (making γ or κ irrelevant), the resulting three-parameter search ($\Delta\chi_{ax}$, α, and β) yields: $\Delta\chi_{ax} = 2.40 \times 10^{-8}$ m^3/mol, $\alpha = 260 \pm 10°$ and $\beta = 4 \pm 1°$; (data not shown; see Supporting Information). This relative insensitivity of the axial anisotropy and its orientation to $\Delta\chi_{rh}$ in *Nm*HO−PH−CN is due to the fact that the heme occupies most of the space that is strongly influenced by the rhombic term in eq 1, such that the δ_{dip} for nonligated residues are reasonably well modeled by a solely $\Delta\chi_{ax}$ value insignificantly different from the true $\Delta\chi_{ax}$. It is reasonable that $\Delta\chi_{ax}$ will similarly dominate the dipolar shifts in *Nm*HO−PH−OH.

Using the δ_{dip}(obs) for assigned protons for *Nm*HO−PH−OH listed in Table 2 as input for a least-squares determination, of initially $\Delta\chi_{ax}$ ($\Delta\chi_{rh} = 0$, $\alpha = \beta = 0$) normal to the heme, yielded a good fit with $\Delta\chi_{ax} = 1.04 \pm 0.10 \times 10^{-8}$ m^3/mol (not shown). Relaxing the restriction of the major magnetic axis normal to the heme, the three-parameter fit ($\Delta\chi_{ax}$, α, β) yielded essentially the same $\Delta\chi_{ax} = 1.05 \pm 0.10 \times 10^{-8}$ m^3/mol, with a very small tilt $\beta = 4 \pm 1°$ in a direction with $\alpha = 260 \pm 15°$, an inconsequentially reduced residual error function, and a reasonable correlation between δ_{dip}(obs) and δ_{dip}(calc), as shown in Figure 9. Moreover, the optimized magnetic axes do not predict any hyperfine shifted signal which should partially resolved either on the diamagnetic envelope edges or in the small window between the aromatic and aliphatic protons. Hence, we conclude that the magnetic anisotropy of *Nm*HO−PH−OH is predominantly axial, clearly positive in sign, and ~40% of the magnitude of that in *Nm*HO−PH−CN.[34] These results are consistent only with the primary population of the d_π (or $d^2_{xy}(d_{xz},d_{yz})^3$) ground state.

Influence on H-Bond Strength. Low-field bias of labile proton diamagnetic chemical shifts has been shown to correlate with H-bond length and, hence, H-bond strength.[59,60] However, to compare the different derivatives of *Nm*HO, the observed chemical shift, δ_{DSS}(obs), must be corrected for the contribution from the paramagnetism, δ_{dip}(calc), obtained via the magnetic axes derived above. Hence, δ_{DSS}(dia*) is obtained via:

$$\delta_{DSS}(\text{dia*}) = \delta_{DSS}(\text{obs}) - \delta_{dip}(\text{calc}) \qquad (4)$$

where δ_{DSS}(dia*) reflects the H-bond effects. The δ_{DSS}(obs) and δ_{DSS}(dia*) values obtained for assigned labile protons in *Nm*HO−PH−OH are listed in Table 1, where they can be

Table 1. Comparison of Labile Proton Chemical Shifts for *Nm*HO−PH−OH and *Nm*HO−PH−H_2O

	*Nm*HO–PH–OH			NmHO–PH–H_2O	comparison	
	δ_{DSS} (obs)[a]	δ_{dip} (calc)[b]	δ_{DSS} (dia*)[c]	δ_{DSS} (dia*)[d]	$\Delta\delta_{dip}$ (calc)[e]	$\Delta\delta_{DSS}$ (dia*)[f]
			Peptide NHs			
Ala12	9.15	−0.09	9.24	9.31	0.29	0.07
Tyr112	8.36	−0.22	8.58	8.68	0.72	0.10
Cys113	7.75	−0.40	8.15	8.40	1.35	0.25
Ala114	8.70	−0.40	9.10	9.00	1.33	−0.10
Gln115	9.40	−0.27	9.67	9.50	0.78	−0.17
Gly138	10.30	0.05	10.25	10.28	−0.18	0.03
Ala139	7.67	0.08	7.59	7.58	−0.30	−0.01
Arg140	12.10	0.11	11.99	12.04	−0.37	0.05
His141	10.78	0.15	10.63	10.75	−0.52	0.12
Leu142	6.82	0.27	6.55	6.68	−0.92	0.13
Asp147	10.70	0.12	10.58	10.60	−0.39	0.02
Ala180	8.39	−0.11	8.50	8.42	0.44	−0.08
Phe181	8.04	−0.12	8.16	8.03	0.57	−0.13
Ala182	7.77	−0.02	7.79	7.97	0.20	0.12
Phe183	8.61	−0.08	8.69	8.65	0.35	−0.04
Tyr184	8.15	−0.19	8.34	8.51	0.73	0.17
			Side chain NHs			
Gln49 $N_{\epsilon 1}H$	9.70	0.14	9.56	9.76	−0.72	0.20
Gln49 $N_{\epsilon 2}H$	6.97	0.17	6.80	7.04	−1.00	0.26
His53 $N_{\epsilon 1}H$	12.07	0.10	11.97	11.48	−0.66	−0.51
Trp110 $N_{\epsilon}H$	11.60	−0.08	11.68	11.70	0.29	0.02
His141 $N_{\delta 1}H$	13.35	0.12	13.23	13.24	−0.48	0.01
Trp153 $N_{\epsilon}H$	9.40	−0.36	9.76	10.54	1.25	0.82

[a] δ_{DSS}(obs), in ppm, referenced to DSS via the solvent signal, in ^1H_2O, 100 mM bicarbonate at 25 °C and pH 10.2. [b] Dipolar shift predicted by the determined magnetic axes described in Figure 8. [c] The diamagnetic shift that reflects H-bonding differences between OH^- and H_2O complexes, as given by eq 4. [d] As reported previously.[50] [e] $\Delta\delta_{dip}$(calc) = δ_{dip}(calc; *Nm*HO−PH−H_2O) − δ_{dip}(calc; *Nm*HO−PH−OH). [f] $\Delta\delta_{DSS}$(dia*) = δ_{DSS}(dia*; *Nm*HO−PH−H_2O) − δ_{DSS}(dia*; *Nm*HO−PH−OH), as determined from δ_{DSS}(dia*; *Nm*HO−PH−OH) in eq 4 and δ_{DSS}(dia*; *Nm*HO−PH−H_2O) reported by Liu et al.[50]

compared to previously reported[50] δ_{DSS}(dia*) values for the *Nm*HO−PH−H_2O complex.

Discussion

Resonance Assignments. The dominance of exchange cross-peaks at all pHs at which there is more than ∼10% *Nm*HO−PH−OH dramatically limits the de novo assignment of residues within the *Nm*HO−PH−OH complex at any pH where the sample is reasonably stable to degradation over 24 h. However, because the exchange cross-peaks appear only upon increasing the pH above pH 7.0, it is possible to transfer to *Nm*HO−PH−OH, by exchange, the assignment of peaks previously[50] assigned that are resolved or exhibit large dipolar shifts in the *Nm*HO−PH−H_2O complexes.[50] This naturally restricts residue assignments in *Nm*HO−PH−OH to those residues that in *Nm*HO−PH−H_2O exhibited significant dipolar shifts or exhibited stronger than usual H-bonds. Fortunately, these are precisely the target residues for describing the magnetic properties and H-bond interactions in *Nm*HO−PH−OH. Although the assignment of residues in the homologous *Pa*HO complex has not been reported, the heme signals exhibit[40] similar slow exchange between the H_2O and OH^- complexes, such that a similar assignment strategy would be applicable.

Table 2. Chemical and Dipolar Shift Data for Strongly Dipolar-Shifted Residues in *Nm*HO−PH−OH, *Nm*HO−PH−H_2O and *Nm*HO−PH−CN

		*Nm*HO–PH–OH			*Nm*HO–PH–H_2O	*Nm*HO–PH–CN
		δ_{DSS} (obs)[a]	δ_{DSS} (dia)[b]	δ_{dip} (obs)[c]	δ_{dip} (obs)[d]	δ_{dip} (obs)[e]
Ala12	$C_{\alpha}H$	3.39	3.82	−0.42	0.21	−0.52
	$C_{\beta}H_3$	1.24	1.45	−0.23	0.42	−0.47
Thr20	$C_{\gamma}H_3$	1.30	0.09	1.21	−1.76	2.18
Ala21	$C_{\beta}H_3$	1.47	0.80	0.67	−0.65	1.24
Val22	$C_{\gamma 1}H_3$	0.70	−0.07	0.77	−0.57	1.57
	$C_{\gamma 2}H_3$	0.98	0.36	0.34	−0.48	1.06
Asp24	$C_{\beta 1}H$	2.82	2.14	0.58	−2.51	1.51
	$C_{\beta 2}H$	3.08	2.00	1.08	−2.60	2.30
Phe52	$C_{\epsilon}Hs$	7.43	7.53	−0.10	0.62	−0.82
	$C_{\zeta}H$	7.31	7.55	−0.24	1.00	−0.15
Tyr112	$C_{\delta}Hs$	6.90	7.37	−0.47	0.31	−1.16
	$C_{\epsilon}Hs$	–	–	–	1.00	−1.15
Cys113	$C_{\beta 1}H$	2.72	3.05	−0.31	1.31	−0.71
	$C_{\beta 2}H$	2.76	3.29	−0.35	1.01	−0.64
Asn118	$C_{\beta 1}H$	3.12	2.42	−0.70	−2.70	1.50
	$C_{\beta 2}H$	3.02	2.30	−0.62	−2.62	1.30
Ala121	$C_{\beta}H_3$	2.30	0.70	1.60	−4.10	4.8
Leu142	$C_{\delta 2}H_3$	0.80	0.02	0.78	−0.77	(1.88)[f]
	$C_{\gamma}H$	0.05	0.00	0.05	−0.85	(0.94)
Trp153	$C_{\delta 1}H$	6.95	7.11	−0.16	0.71	−0.14
Val157	$C_{\alpha}H$	2.85	3.24	−0.39	(0.30)[g]	−0.36
	$C_{\beta}H$	1.55	−2.01	−0.46	(0.26)	−0.35
	$C_{\gamma 1}H_3$	0.37	1.02	−0.65	(0.29)	−0.38
	$C_{\gamma 2}H_3$	−0.02	0.12	−0.14	(0.45)	0.55
Phe181	$C_{\beta 1}H$	3.57	3.12	0.43	−0.17	0.15
	$C_{\beta 2}H$	3.03	2.84	0.18	0.32	0.73
Phe183	$C_{\alpha}H$	4.53	4.26	−0.27	0.25	(−0.15)[g]
	$C_{\beta 1}H$	3.68	3.37	−0.29	0.30	(−0.22)
	$C_{\beta 2}H$	3.42	3.26	−0.16	0.40	(−0.14)
	$C_{\delta}Hs$	7.64	7.75	−0.11	0.21	−0.61
	$C_{\epsilon}Hs$	7.37	7.62	−0.25	0.02	−0.26
Tyr184	$C_{\delta}Hs$	6.18	6.92	−0.74	0.62	−1.13
	$C_{\epsilon}Hs$	6.48	7.07	−0.63	1.00	−1.15

[a] δ_{DSS}(obs) in ppm referenced to DSS via the solvent resonance, in ^2H_2O at pH 9.1, 100 mM in bicarbonate at 25 °C. [b] Diamagnetic chemical shift in ppm, at 25 °C, calculated by the ShiftX program[56] and the *Nm*HO−PH−H_2O crystal structure. [c] Given by eq 3. [d] As reported in ref 50 and converted to δ_{dip}(obs) using eq 3 and the same δ_{DSS}(dia) as for *Nm*HO−PH−OH. [e] As previously reported in ref 34 and converted to δ_{dip}(obs) by eq 3 and the same δ_{DSS}(dia) as for *Nm*HO−PH−OH. [f] Not assigned in *Nm*HO−PH−CN; given in parentheses is the δ_{dip}(calc) from the published magnetic axes. [34] [g] Not assigned in *Nm*HO−PH−H_2O; given in parentheses is the δ_{dip}(calc) from the published magnetic axes.[50]

Thermodynamics/Dynamics of the $H_2O \Leftrightarrow OH^-$ Transition. The integration of heme methyl peaks in the H_2O and OH^- complexes leads to the Henderson−Hasselbach plot in Figure 4. Integration of a high-spin and low-spin resolved methyl peaks indicates that a 1:1 population occurs at pH 9.8 in ^2H_2O (uncorrected for isotope effect) and at about 0.4 units lower in ^1H_2O, pH ∼9.4 (based on integration of the pH 10.2 spectra in ^1H_2O). The apparent p*K* for *Nm*HO is some 1.5−1.8 units higher than values reported for the homologous *Pa*HO complex (∼8.0−8.3).[13,40] The obvious conclusion is that the H_2O complex is stabilized, and/or the OH^- complex is destabilized,[41] in *Nm*HO relative to *Pa*HO substrate complexes. Comparison of the axial field strengths via $\Delta\chi_{ax}$ and *D*,[61] the zero-field splitting parameter,[50] in the two HO−PH−H_2O complexes would shed some light on potential differences in ligated water H-bonding with the protein matrix for the high-spin complexes of *Pa*HO and *Nm*HO. Such data are available for the *Nm*HO complex[50]

(59) Wagner, G.; Pardi, A.; Wüthrich, K. *J. Am. Chem. Soc.* **1983**, *105*, 5948−5949.
(60) Harris, T. K.; Mildvan, A. S. *Proteins: Struct., Funct., Genet.* **1999**, *35*, 275−282.
(61) Brackett, G. C.; Richards, D. L.; Caughey, W. S. *J. Chem. Phys.* **1971**, *54*, 4383−4401.

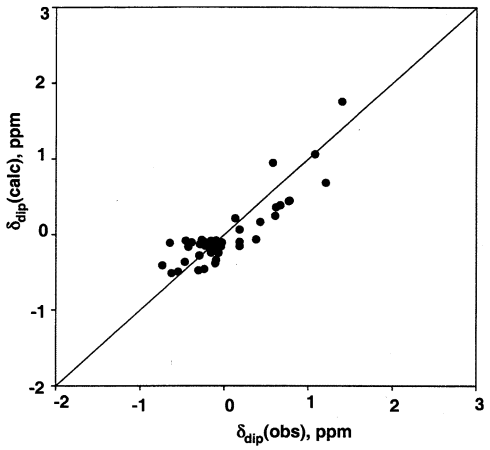

Figure 9. Plot of δ_{dip}(obs) versus δ_{dip}(calc) for the optimized anisotropy and orientation of axially symmetric paramagnetic susceptibility tensor χ of *Nm*HO−PH−OH at 25 °C, with $\alpha = 260 \pm 15°$, $\beta = 4 \pm 1°$, and $\Delta\chi_{ax} = 1.04 \pm 0.14 \times 10^{-8}$ m^3/mol. The residual error function, $F/n = 0.20$ ppm^2.

but not yet for the *Pa*HO complex. The estimated rate of exchange $<10^3$ s^{-1} for the *Nm*HO−PH complex is somewhat slower than estimated for the *Pa*HO−PH complex.[40] Similarly, slow exchange has been reported for the *Pa*HO−PH−H_2O/OH pair,[40] but such slow echange is not typical for all such HO complexes, as hHO exhibits fast exchange.[62]

Magnetic Properties and Orbital Ground State for *Nm*HO−PH−OH. The comparison of the sign of δ_{dip}(obs) for assigned signals of *Nm*HO−PH−OH with the reported sign of δ_{dip}(obs) for $S = {}^1/_2$, d_π *Nm*HO−PH−CN[34] ($\Delta\chi_{ax} > 0$), and $S = {}^5/_2$ *Nm*HO−PH−H_2O[50] ($\Delta\chi_{ax} < 0$) in Table 2 establishes that the axial anisotropy of *Nm*HO−PH−OH is clearly positive. Quantitation of $\Delta\chi_{ax}$ leads to $\Delta\chi_{ax} = 1.04 \pm 0.10 \times 10^{-8}$ m^3/mol. The retained sign but reduced magnitude of the axial anisotropy in *Nm*HO−PH−CN relative to *Nm*HO−PH−OH is consistent with the pattern of the *g*-values in the EPR spectra of the same metglobin complexes.[45] The sign and magnitude of $\Delta\chi_{ax}$ in *Nm*HO−PH−OH therefore support only a predominantly d_π orbital ground state[38,45]

The resolved *Nm*HO−PH−OH heme $3CH_3$ and $8CH_3$ peaks exhibit deviations from the general Curie behavior of the low-field methyl peak in the d_π orbital ground state of low-spin cyano-ferrihemoprotein[49,63,64] complexes. However, hydroxide is a significantly weaker axial field strength ligand than cyanide, and the majority of metglobin hydroxide complexes with the dominant d_π, $S = {}^1/_2$ ground state exhibit similar deviations from Curie behavior[49] because of the weak thermal population of the high-spin ferric state with its much larger methyl contact shifts.

The present results for *Nm*HO−PH−OH with a d_π ground state are in contrast to the d_{xy} orbital ground state proposed[6,40] for the homologous *Pa*HO−PH−OH complex on the basis of the ^{13}C contact shift pattern of the PH substrate. The significant difference in the p*K*s for the acid−alkaline transition in *Pa*HO and *Nm*HO complexes would allow for significant differences in the effective axial field strength of the OH^- ligand, such that different orbital ground states could, in principle, be populated for the two complexes. The relative values for the p*K*s for the two complexes are consistent with, but not proof for, stronger H-bond stabilization of the ligated OH^- by proton donation by a nonligated water in *Pa*HO than *Nm*HO (see Figure 1C). At this time, the ^{13}C analysis of PH contact shifts[40] has not been performed on *Nm*HO−PH−OH, and the sign and magnitude of the axial anisotropy have not been reported for *Pa*HO−PH−OH. Similar studies on both HOs may resolve this apparent paradox. The present data, however, indicate emphatically that the d_{xy} orbital ground state of the HO−PH−OH complex is clearly *not a signature of the general distal HO environment*.

Dynamic Stability of *Nm*HO−PH−OH. It is remarkable that essentially all of the labile proton signals characterized[50] at pH 7.0 in *Nm*HO−PH−H_2O are still detectable at pH 10.2, because they usually exhibit base-catalyzed exchange.[65] Even more remarkable is the observation that saturation factors in 3:9:19 difference-spectra[52] between on-resonance and off-resonance saturation of the water signal at pH 10.2 (not shown; see Supporting Information) leads to small, and essentially the same (or smaller), saturation factors at pH 10.2 as observed at pH 7.0, where their exchange rate with bulk solvent was shown to be extremely slow.[34] Thus, the high dynamic stability, as reflected in very slow exchange rates of NHs, observed near neutral pH appears to be retained even in strongly alkaline medium.

Effect of H_2O to OH^- Conversion on the Distal H-bond Network: Corrections of δ_{DSS}(obs) for δ_{dip}(calc) for assigned *Nm*HO−PH−OH labile protons are listed in Table 1. Also included are δ_{dip}(calc) values for *Nm*HO−PH−OH, which allow determination of δ_{DSS}(dia*), and the differences in δ_{dip}(calc) between the two complexes: $\Delta\delta_{dip}$(calc) = δ_{dip}(calc:*Nm*HO−PH−H_2O) − δ_{dip}(calc:*Nm*HO−PH−OH), where δ_{dip}(calc:*Nm*HO−PH−H_2O) values have been published previously,[50] and δ_{dip}(calc) for *Nm*HO−PH−OH are estimated by the magnetic axes described above. It must be noted that, because both the *Nm*HO−PH−H_2O and *Nm*HO−PH−OH magnetic axes determinations are based on only $\Delta\chi_{ax} \neq 0$ (i.e., $\Delta\chi_{rh} = 0$) and the magnetic axes for *Nm*HO−PH−OH on the basis of significantly fewer experimental δ_{dip}(obs) than from *Nm*HO−PH−H_2O,[50] the uncertainties of $\Delta\delta_{dip}$(calc) increase with increasing δ_{dip}(calc) for either complex. Hence, we conclude that differences in δ_{DSS}(dia*) between the H_2O and OH^- complex are significant only if this difference is comparable to the magnitude of $\Delta\delta_{dip}$(calc).

Inspection of Table 1 shows that, although δ_{DSS}(obs) differs by as much as 1.6 ppm between the two complexes, correction for δ_{dip}(calc) for each complex reduces the difference in δ_{DSS}(dia*) to well under 0.2 ppm for all but a few labile protons. Hence the strength of the majority of the H-bonds is strongly conserved upon deprotonating the axial water. Among those NHs with significant (>0.2 ppm) differences in δ_{DSS}(dia*) in Table 1, Gln49 N_ϵHs, and Cys113 NH each exhibits large $|\Delta\delta_{dip}$(calc)| ~1.0−1.3, rendering the interpretation of $\Delta\delta_{DSS}$(dia*) questionable. On the other hand, His53 $N_{\epsilon 1}$H and Trp153 N_ϵH exhibit lower-field bias in the OH^- than H_2O complex, by amounts that are close to the $\Delta\delta_{dip}$(calc) and, hence, can be considered significant. The data in Table 1 lead to the conclusion that the diamagnetic chemical shift, and hence H-bond donor

(62) Zhu, W; Ogura, H; Wong, J.-L.; Ortiz de Montellano, P. R.; La Mar, G. N.. Unpublished data.
(63) Turner, D. L. *J. Magn. Reson.* **1993**, *Series A 104*, 197−202.
(64) Shokhirev, N. V.; Walker, F. A. *J. Phys. Chem.* **1995**, *99*, 17795−17804.
(65) Englander, S. W.; Kallenbach, N. R. *Quart. Rev. Biophys.* **1984**, *16*, 521−655.

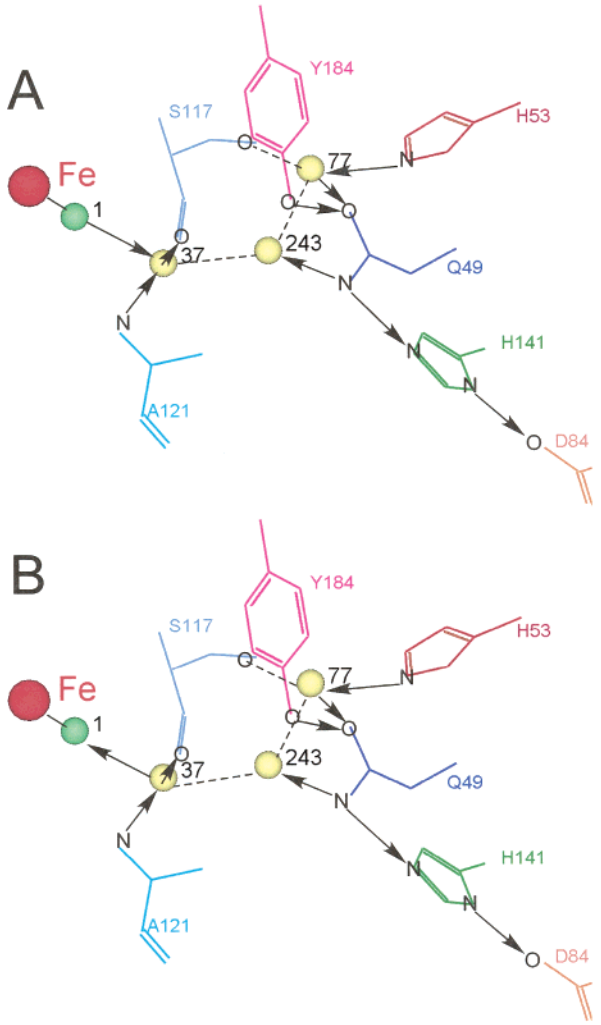

Figure 10. (A) Schematic structure of the distal cavity of *Nm*HO−PH−H_2O showing the relative position of the ligated water, H_2O #1 (green sphere), the three conserved catalytically relevant, nonligated water molecules, H_2O #243, H_2O #37, and H_2O #77 (yellow spheres), and several key residues involved in the H-bond stabilization of these water molecules based on the *Nm*HO−PH−H_2O crystal structure and the previously documented 180° rotation about the $\beta-\gamma$ bond for the Gln49 and His53 side chain.[34,50] The direction of H-bonds (donor → acceptor) are shown in solid arrows between the two heteroatoms. For cases where neither the crystal structure nor solution ^{1}H NMR uniquely locates the position of the proton, and hence the direction of the H-bond cannot be definitively determined, the presence of the H-bond is shown as a dashed line. (B) Structure of *Nm*HO−PH−H_2O retained for the *Nm*HO−PH−OH complex, except that the H-bond direction between H_2O #1 and H_2O #37 is reversed from that in A. The changed direction of the axial ligand (green sphere) in converting H_2O (A) to OH (B) is consistent with the His53 $N_{\epsilon 1}H$ serving as a strong donor upon deprotonating the water.

strengths for His53 $N_{\epsilon 1}H$ and Trp153 $N_\epsilon H$, is significantly modulated by the $H_2O \leftrightarrow OH^-$ conversion, with both H-bond donor strengths slightly greater in the OH^- than H_2O complex.

Figure 10 presents a schematic of the active site of *Nm*HO−PH−H_2O[14] that depicts the ligated H_2O (Figure 10A) or OH^- (Figure 10B) (both green spheres) and the three noncoordinated, catalytically implicated ordered water molecules (yellow spheres), as well as the residues (specifically His53) that interact directly, or indirectly, with these water molecules. The side chains of both Gln49 and His53 are rotated 180° about the $\beta-\gamma$ bonds from that in the crystal structures,[14,15] as confirmed by solution NOESY cross-peaks in both *Nm*HO−PH−CN[34] and *Nm*HO−PH−H_2O.[50] Arrows depict H-bond direction for cases where the position of the donor and acceptor atoms are clear. Dashed lines represent the other H-bonds for which it is not possible, based on either crystallography or ^{1}H NMR, to uniquely ascertain the direction of the proton donation. Conversion of the necessarily H-bond donor (Figures 1B and 10A) ligated water #1 to a necessarily H-bond acceptor hydroxide molecule (Figures 1C and 10B) logically leads to a stronger H-bond donation by His53 $N_{\epsilon 1}H$ for the ligated OH^- as observed.

Trp153 $N_\epsilon H$ in *Nm*HO−PH−H_2O serves as a H-bond donor primarily to an ordered H_2O molecule #44, which, in turn, H-bonds to another ordered H_2O molecule #32 that is a donor to the carboxylate of the 6-propionate.[14] Increasing the negative charge on the heme by deprotonating the axial water could lead to the propionate anion carboxylate serving as a stronger H-bond acceptor to the ordered H_2O #32, with the effect further transmitted to the Trp153 $N_\epsilon H$. The δ_{DSS}(dia*) values for Gln49 N_ϵHs chemical shifts, and hence H-bond strength of the side chain, appear also to respond to $H_2O \rightarrow OH^-$ conversion, but the chemical shift difference is much less than the $\Delta\delta_{dip}$(calc). The further quantitation of $\Delta\chi_{rh}$ for *Nm*HO−PH−OH would assist in more accurately defining the change in H-bond strength. Although additional assignments in *Nm*HO−PH−OH by ^{1}H NMR may be problematical due to the high p*K* and the inability to predominantly populate the *Nm*HO−PH−OH complex, the use of electron withdrawing substitutions is known[42−44] to markedly lower the acid−alkaline p*K* and, hence, could allow a complete conversion to the hydroxide complex below pH 10 without danger of degradation at the extreme pH. Similar ^{1}H NMR studies of the hydroxide complex of a formyl-substituted substrate are planned.

The data show that the state of the axial water is transmitted to the His53 side chain $N_{\epsilon 1}H$ some 10 Å from the iron. Because the primary interaction of the iron ligand is with one (#37) of the ordered water molecules, which is linked to His53 by an additional two ordered water molecules (#243 and #77), it is reasonable that this "link" between the ligand and His53 is transmitted via the water chain. The small effect on His53 $N_{\epsilon 1}H$, and the absence of clear perturbations of other H-bonds in the distal network (i.e., His141, Gln49) by the H_2O to OH^- conversion may be considered surprising, in view of the dramatic acid/base properties of the alternate heme iron ligands. However, each of these residues, as well as the catalytic water molecules shown in Figure 10, are members of a much more extended network of H-bonds and ordered water molecules[15,34] such that this highly coupled network may compensate for a single strong perturbation within the network. The further characterization of the H-bond/ordered water network must await planned ^{15}N-labeling of *Nm*HO.

Conclusions

The assignment of active site residues in ferric, low-spin, *Nm*HO−PH−OH reveals a pattern of dipolar shifts for active-site residues that is consistent with only positive axial anisotropy for the paramagnetic susceptibility tensor. Quantitation of the tensor yields an axial anisotropy with ~40% of the magnitude found in the well-characterized ferric, low-spin *Nm*HO−PH−CN complex.[34] Hence, the dominant orbital ground state for *Nm*HO−PH−OH is the common d_π, and not the unusual d_{xy} orbital state suggested to be a signature of the HO active site.

The conversion of the H-bond donor ligated water to the H-bond acceptor ligated hydroxide leads to a detectable strengthening of the His53 side chain H-bond, which is linked to the ligated water/hydroxide through three ordered water molecules.

Acknowledgment. This work was supported, in part, by the National Institutes of Health, GM 62830 (G.N.L.), HL 16087 (G.N.L.), and a grant-in-aid for Scientific Research (16570102) from the Ministry of Education and Sports, Science and Teaching, Japan (T.Y.)

Supporting Information Available: Four figures (partially relaxed spectra for *Nm*HO−PH−OH, Curie plot for heme methyls and comparison of magnetic axes determination for *Nm*HO−PH−CN with and without considerations of rhombic anisotropies, and labile proton saturation factors) and one Table (chemical shifts for assigned *Nm*HO−PH−OH residues). This material is available free of charge via the Internet at http://pubs.acs.org.

JA0584626